Cellular and Molecular Bioengineering, Vol. 5, No. 3, September 2012 (© 2012) pp. 307–319
DOI: 10.1007/s12195-012-0237-8

Cell Adhesion on Micro-Structured Fibronectin Gradients Fabricated by Multiphoton Excited Photochemistry

XIYI CHEN,[1] YUAN-DENG SU,[2] VISAR AJETI,[1] SHEAN-JEN CHEN,[2] and PAUL J. CAMPAGNOLA[1]

[1]Department of Biomedical Engineering, University of Wisconsin-Madison, Madison, WI 53717, USA; and [2]Department of Engineering Science, National Cheng Kung University, Tainan, Taiwan

(*Received 11 February 2011; accepted 20 June 2012; published online 3 July 2012*)

Associate Editor Joyce Wong oversaw the review of this article.

Abstract—Concentration gradients of ECM proteins play active roles in many areas of cell biology including wound healing and metastasis. They may also form the basis of tissue engineering scaffolds, as these can direct cell adhesion and migration and promote new matrix synthesis. To better understand cell–matrix interactions on attractive gradients, we have used multiphoton excited (MPE) photochemistry to fabricate covalently linked micro-structured gradients from fibronectin (FN). The gradient design is comprised of a parallel series of individual linear gradients with overall dimensions of approximately 800 × 800 μm, where a linear dynamic range of nearly 10-fold in concentration was achieved. The adhesion dynamics of 3T3 fibroblasts were investigated, where the cell morphology and actin cytoskeleton became increasingly elongated and aligned with the direction of the gradient at increasing protein concentration. Moreover, the cell morphologies are distinct when adhered to regions of differing FN concentration but with similar topography. These results show that the fabrication approach allows investigating the roles of contact guidance and ECM cues on the cell–matrix interactions. We suggest this design overcomes some of the limitations with other fabrication methods, especially in terms of 3D patterning capabilities, and will serve as a new tool to study cell–matrix interactions.

Keywords—ECM, Crosslinking, Contact guidance, Morphology, Cytoskeleton.

INTRODUCTION

It is now well-appreciated that spatial concentration and stiffness gradients of bioactive molecules in the extracellular matrix (ECM) play important roles in several areas of cell biology, including morphogenesis, wound healing, and metastasis.[36] For example, concentration gradients of matrix proteins that direct cell adhesion and migration may promote new matrix synthesis *in vivo* as recruitment of fibroblasts in response to damage is an early step in process of regeneration/repair. Thus, technologies and methods that can afford precise positioning of ECM components in gradients with well-defined concentrations could find broad utility, in terms of as tools to study cell–matrix interactions as well as having potential use in tissue engineering applications.

To address this need, several labs have reported approaches to gradient fabrication of differing complexity to examine a range of biological problems. For example, sophisticated microfluidic approaches have been employed to create concentration gradients to study cell adhesion/migration dynamics.[6,13,18,19,21,33] Microcontact printing has also been used to create 2D concentration gradients for axonal outgrowth studies, where these have been created in a variety of geometries with feature sizes ranging from sub-micron to tens of microns.[15,39] A primary advantage of this approach is that it affords changing feature size and spacing to study the resulting cell response. More recent schemes have used multistep optical and surface modification approaches[4,25] or have utilized non-native photoactivatable peptides[40] to add flexibility in synthesizing gradients from a wider range of starting materials.

To make models that may be more biomimetic in terms of the underlying substrate mechanical characteristics, several approaches have been employed to functionalize hydrogels to create stiffness and concentration gradients. For example, Wong and co-workers used microfluidics to create stiffness gradients from polyacrylamide gels to investigate durotaxis of vascular smooth muscle cells, where the substrates were coated with collagen to induce cell adhesion.[20] Analogously, surface concentration gradients of bioactive

Address correspondence to Paul J. Campagnola, Department of Biomedical Engineering, University of Wisconsin-Madison, Madison, WI 53717, USA. Electronic mail: pcampagnola@wisc.edu
Xiyi Chen and Yuan-Deng Su contributed equally to this work.

molecules on soft substrates of constant stiffness have also been created. For example, West and coworkers showed that hydrogels whose surfaces were modified with continuous gradients (overall several mms) of PEG-conjugated growth factors[12] and RGD binding domains[11] were highly effective in directing smooth muscle cell and fibroblast alignment and migration.

As demonstrated by the previous examples, 2D modifications of hard surfaces and hydrogels have been used to create concentration and stiffness gradients and have become established, powerful components in the toolbox to study cell–matrix interactions. To yield still greater capabilities, it would be advantageous to create concentration gradients directly from native full-length ECM proteins that are crosslinked together, as these may be more biomimetic. More importantly, additional power will come from incorporating 3D nano/microscale topographic features in the gradient design since ECM proteins *in vivo* are covalently assembled into nano/microstructured fibril/fibers which have binding domains that are recognized by cell integrins.

Here we begin to address this challenge by presenting a new approach to synthesizing covalently linked micro-structured ECM protein gradients through the use of multiphoton excited (MPE) photochemistry. This photochemical process is analogous to two-photon excited (TPE) fluorescence microscopy, where the excitation, and here, the fabrication, is confined to the focal volume, resulting in intrinsic 3D capabilities and concurrently affording sub-micron feature sizes.[2,9,22,24,26,30,31,35] Freeform 3D capabilities with submicron feature sizes are not currently possible by microfluidic and microcontact printing methods. Moreover, the crosslinked protein concentration achieved by MPE can be well controlled by tuning the laser exposure.[1] Because of these attributes, the MPE process offers great flexibility for the fabrication of synthetic ECMs in terms of composition and topography. Our previous efforts using this technology have been directed at fabricating and characterizing scaffolds from several ECM proteins and also investigating some aspects of the concomitant cell response.[1,2,29] For example, we characterized the initial adhesion and spreading response (3 h) of dermal fibroblasts on micropatterned crosslinked fibronectin (FN), fibrinogen, collagen, and BSA fibers.[2,29] By studying the resulting morphological response of fibroblasts to linear structures with the same topography and concentration, we have shown how topography (i.e., contact guidance) and ECM cues, together and separately, affect cell morphology. More recently, we also used this approach to investigate the adhesion/migration dynamics of ovarian cancer cells as a function of metastatic potential.[8]

Unexamined questions include how cells respond to ECM protein concentration and/or local changes therein, and/or changes in topography, where all these conditions may occur *in vivo*. To the best of our knowledge, these issues have not been studied with 3D micropatterned covalently linked proteins. These issues cannot be well-addressed by 2 dimensional approaches, where, for example, many previous studies employed monolayers or "islands" of cell-adhesive surface regions created through soft lithography approaches.[10,16,34] To better understand these cell–matrix interactions we employ MPE fabricated FN concentration gradients to investigate the adhesion and spreading dynamics of 3T3 fibroblasts both in terms of the resulting morphology and the cytoskeletal response. This represents a good test system as the fibroblast integrin-FN interactions have been well-characterized on surfaces.[16] Through this approach we show how alignment and orientation effects become more pronounced with increasing concentration.

METHODS

Fabrication Instrument and Photochemistry

The multiphoton fabrication instrument/microscope has been described in detail previously.[35] Briefly, the multiphoton photochemistry is induced by a femtosecond titanium sapphire laser that is coupled to a purpose-built laser scanning microscope system mounted on an upright stand. The scanning/acquisition software is written in LabVIEW and is freely available upon request. One and two-photon photochemistry of the Rose Bengal photoactivator used for protein crosslinking has been described previously.[7,28,30] Here two-photon excitation was employed at 780 nm with an average power at the focus of 100 mW when using a 0.5 numerical aperture (NA) lens.

Sample Preparation

The FN gradients and linear structures (or "fibers") of constant concentration are fabricated on a microscope slide, where a self-assembled organosilane monolayer (octadecyltrichlorosilane; ODTS) is coated with a monolayer of BSA (10 mg/mL) to form the base for the crosslinked FN.[2] We use "fiber" purely as a means to describe the morphology of the fabricated constructs, where this is intended to stress the 3D nature and does not imply any supramolecular characteristics. As reported previously,[29] the BSA is used as a non-specific surface to compare the adhesion dynamics of cells adhered to and away from the crosslinked FN. By fluorescence microscopy imaging of the BSA (~1% concentration labeled

with Texas Red), we found this background was stable over the 72 h period in which cell adhesion measurements were performed. The fabrication solution consisted of 0.5 mg/mL FN (mouse) and 2.5 mM Rose Bengal in water and was confined in a small circular rubber chamber seated on top of the self-assembled BSA monolayer.[2] After fabrication, the structures were washed with deionized water, rinsed with PBS pH 7.4 which contained 400 μg/mL penicillin and 400 μg/mL streptomycin under sterile conditions, and kept hydrated for cell plating.

Gradient Design and Characterization

As a compromise between field size and resolution a 10 × 0.5 NA objective was used for fabrication which yielded a field of view of 800 μm. The overall gradient structure consisted of a series of individual linear gradients where each was 800 μm in length. These were designed such that the point density of the protein fabrication increased linearly from 0.01 to 0.4 point/μm while the laser power was maintained at a constant average power of 100 mW at the focus. At the low concentration regions, the crosslinked FN is localized into discrete points, which become continuous at the higher point densities, which occurs at approximately 0.2 point/μm. Higher point densities then result in increased local concentrations with the same topography. As previously determined by higher resolution optical microscopy measurements, this optical setup yields fiber sizes of approximately 700 nm in diameter and 2 μm in height.[35]

The laser was scanned with the galvo-mirrors at a much lower low speed (500 Hz) than that typically used for image acquisition on a confocal microscope (~10 kHz). The slow speed was required for accurate beam positioning to overcome the error arising from intrinsic inertia of the galvo-mirrors, where this is crucial for the current application so that the resulting fabricated point density is the same as that specified in the scan design. In contrast, designs employing faster scan speeds resulted in nonlinear gradients with limited dynamic range and also yielded non-reproducible patterns. If any small changes in galvo settling times at larger point separations are ignored, the average concentration across the gradient remained linear even where the individual points were discrete. Each individual linear gradient was then separated by 10 μm for an overall width of 800 μm. We have used this spacing previously to study fibroblast and epithelial cell adhesion and spreading.[8,29] Linear patterns of similar dimension were also created at constant point densities of 0.1, 0.2, 0.3 and 0.4 point/μm at constant laser power to elucidate the role of local concentration on the cell adhesion dynamics.

The resulting spatial distribution of FN concentration was determined by immunofluorescence imaging, where the structures were incubated with a primary FN antibody (1:200) and then a secondary fluorescent antibody (1:1000; AlexaFluor 488 conjugated rabbit-anti-mouse IgG). These were imaged by TPE fluorescence at 830 nm, where there was no background fluorescence contribution from any residual entrapped Rose Bengal. We also note that there is no visible residual FN adhered to the BSA surface after washing. To convert the spatial profile obtained by immunofluorescence into protein concentration, we adapted the method reported by Mooney *et al.*[27] Linear FN structures of constant point densities (0.1, 0.2, 0.3 and 0.4 point/μm, respectively) were fabricated to represent different concentration regions (200, 400, 600 and 800 μm) of the gradient and immunostained and imaged as described above. The fluorescence intensity from a standard solution of the secondary fluorescent antibody (0.0133 μM) sealed in a thin chamber (113 μm) was next measured. To calculate the protein concentration in the fibers, dimensions of 0.6 μm in width and 2 μm in height were used to estimate their volume.[35] Scaling of the immunofluorescence intensity along the length of the gradient to the four representative points enabled the determination of the FN concentration profile (Fig. 1b).

Cell Culture

NIH 3T3 cells were cultured on a 24-plate multiwell plate to confluence in Dulbecco's Modified Eagle's medium (DMEM) supplemented with 10% calf bovine serum (CBS) in a humidified incubator at 37 °C in which the CO_2 level was maintained at 5%. The cells were trypsinized and fabricated structures were seeded with ~10,000 cells/mL in DMEM and incubated as above. Maintaining the cells in CBS was required to permit observations over 3 days. The cells were retrieved every 12 h over a 72 h period for phase contrast imaging, and then returned to the incubator. All measurements were performed in triplicate.

Dual Staining for Focal Adhesions and F-actin

36 h post-plating on the fabricated constructs, the cells were fixed for 15 min with 4% formaldehyde, permeabilized with 0.2% Triton X-10, and treated with 1% BSA in PBS to block non-specific binding. For focal adhesion staining, the cells were immunostained for vinculin (anti-vinculin (1:200) and a secondary fluorescent IgG antibody). Cells were stained with Texas Red conjugated phalloidin for F-actin staining (simultaneously with the secondary fluorescent antibody). The dual-stained images were acquired with a

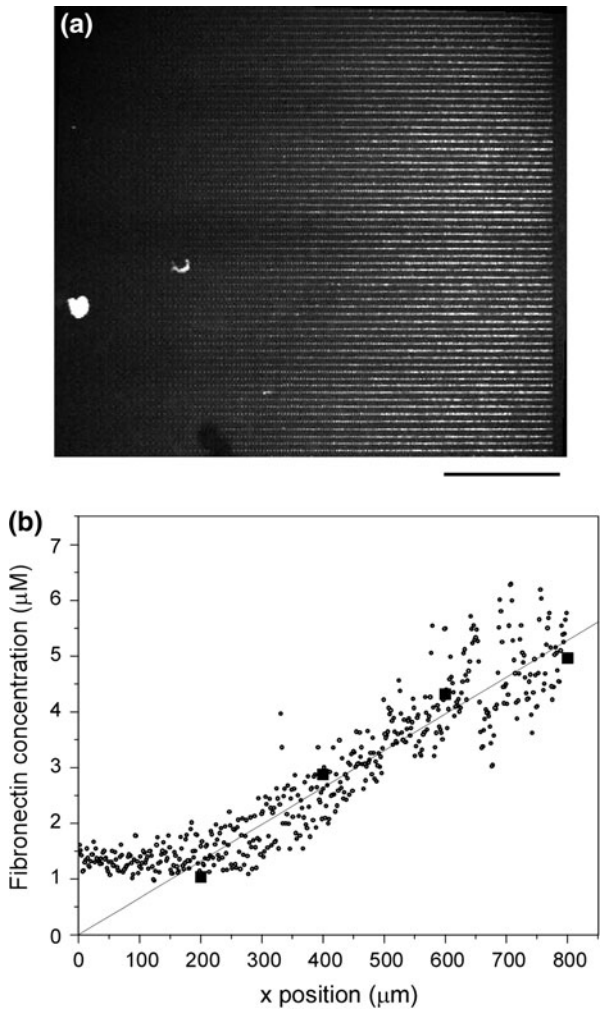

FIGURE 1. (a) Immunofluorescence image of the FN gradient design and (b) plot of the crosslinked FN concentration vs. distance, where the circles are the immunofluorescence from the FN gradient and the squares are the calibration points. This yielded a slope of 6.6 nM/μm. Scale bar = 200 μm.

40× 0.65 NA objective and the corresponding phase contrast images were recorded sequentially.

ImageJ (http://rsb.info.nih.gov/ij) was used to assess the angular distribution of the F-actin distribution in the cells at different FN concentrations. Circular statistical analysis was used to provide a spatial histogram and circular deviation of the stress fiber orientation over the entire cell with respect to the linear FN axis.[23] Here the mean resultant of the stress fibers, R, is a measure of orientation, given by:

$$R = \frac{1}{N}\sqrt{\sum_{j=1}^{N} \sin 2\theta_j + \sum_{j=1}^{N} \cos 2\theta_j} \qquad (1)$$

where N is the number of cells, and θ is the angle of the individual stress fibers.

ImageJ was also used to determine the cell morphological properties with respect to the gradient direction. Here each individual cell was modeled as an ellipse, and the elongation ratio (i.e., ratio of major to minor axes) and the orientation (angle between the long axis of the ellipse and the FN gradient direction) were measured.

Statistical Analysis

Orientation and elongation data are reported as the mean value with the corresponding standard error for different concentration regions of the gradients and also for the patterns of constant concentration. Pair-wise t-tests were used to compare these morphological attributes for adhered cells. The pair-wise Watson U^2 test was used to examine statistical differences in the stress fiber orientation. A standard significance level of $p < 0.05$ was used for all analyses.

RESULTS

Gradient Characterization

We sought to achieve linearity in concentration as this design affords convenience in comparing the effects of concentration on cell response. Figure 1a shows the TPE immunofluorescence of a representative structure, where the FN concentration increases from left to right. The fluorescence intensity across the length was measured and the concentration dependence is given in Fig. 1b (circles). As the first points of the structure in this design were widely separated from the nearest neighbors, the immunofluorescence was comparable to the system noise and fluorescence from residual entrapped Rose Bengal. This led to an apparent constant FN concentration (measured by emission intensity) in the 0–200 μm range, although there is an additional 10-fold concentration range in the region. The first region above the noise threshold was at 200 μm, resulting in a structure 600 μm long for the measurements, over which the dynamic range was approximately 4-fold.

Conversion of the immunofluorescence intensity to crosslinked FN concentration (see "Gradient Design and Characterization" section) yielded a slope of 6.6 nM/μm, where the solid line is a linear fit (R = 0.98) to the four concentration calibration points (solid squares). While there is some scatter in the data, we concluded that a linear change in concentration was achieved through the scan design. We stress that these structures are 3 dimensional and cannot be characterized in terms of surface concentration attributes such as mass/surface area.

We also note that through higher resolution fluorescence imaging (not shown) no change in measured height was found between the low to high concentration points, where at both limits the FWHM was approximately 2 μm. This is because the achieved height (and also diameter) resulting from MPE fabrication does not depend on the integrated laser flux but only on the peak power and the resulting dimensions will correspond to the TPE Point Spread Function (PSF) at that wavelength (in the absence of optical saturation).[3] The measured axial extent is indeed in good agreement with that predicted at the 780 nm laser wavelength[35] and also with our previous findings showing increased laser exposure did not increase the resulting height.[3] In contrast, single photon excited photochemistry has limited axial dependence on the absorption probability and increased flux would be manifested in a simultaneous height increase at higher protein concentrations.

Fibroblast Response to the Gradient

Fibroblast Morphology

We examined whether the FN concentration gradients directed fibroblast spreading. Representative phase contrast images at four timepoints from 5 to 72 h post-plating are given in Figs. 2a–2d in order of increasing time. Figure 2d shows the resulting cell response at 72 h and marked differences are noted in the cell morphology and alignment with increasing FN concentration (from left to right). At increasing concentration the cells become both more elongated and aligned along the linear gradient direction. The spreading response also had a strong temporal dependence. At earlier times [5 (a), 24 (b), and 48 (c) h] the cells had somewhat similar morphology over the length of the gradient. However at 72 h the concentration became highly aligned at the upper concentration limit, suggesting that the contact guidance

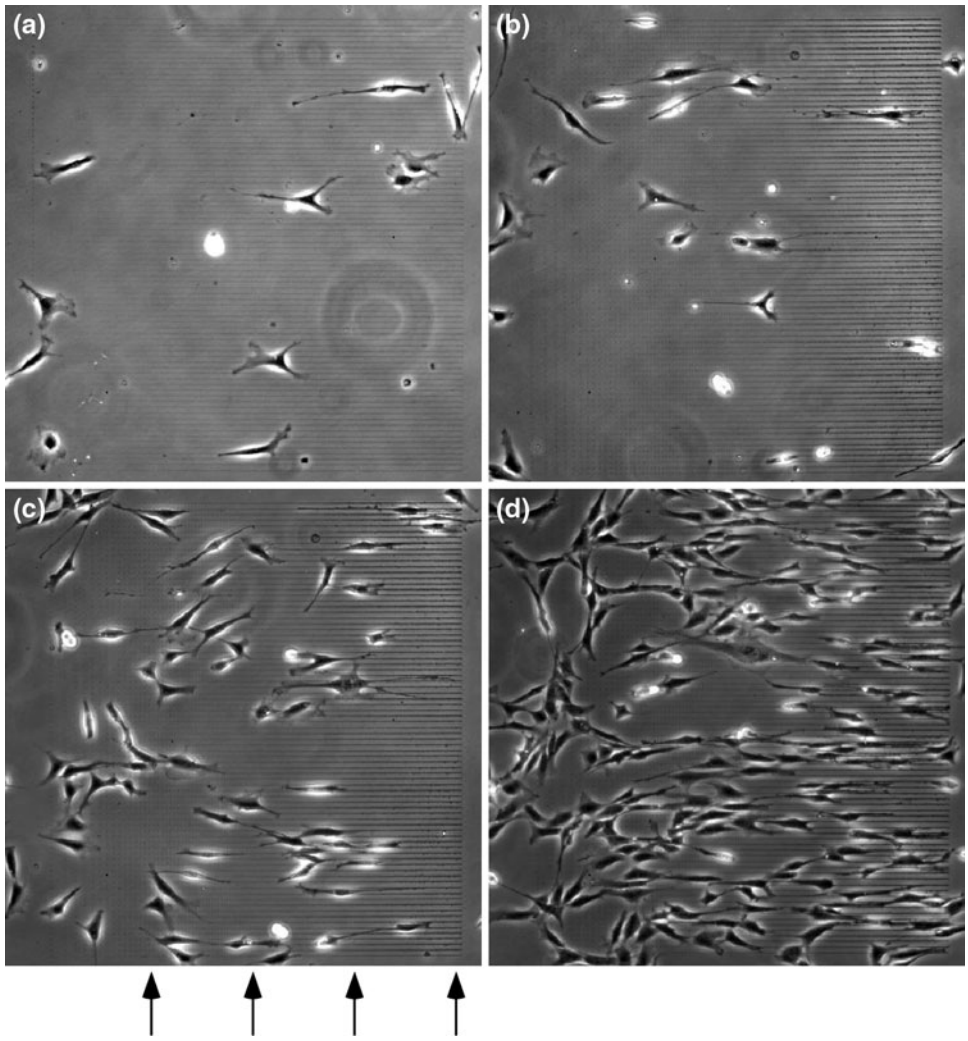

FIGURE 2. Phase contrast images of 3T3 fibroblasts on the FN gradient at four time points of 5 (a), 24 (b), 48 (c), and 72 (d) h post-seeding. The field size is the same as in Fig. 1. The arrows denote the local concentration used for the data in Fig. 4.

provided by the submicron morphology dominated the response at early time and that more time was necessary for the morphology to respond to the increased density of binding sites at the higher FN concentration. We note that in this analysis, we were unable to differentiate cells that had divided against those which had migrated to higher concentrations.

As a control to show that the cell morphology is not simply due to the change in topography in the gradient structure, the fibroblast response was examined on a BSA gradient on a BSA background fabricated with the same design parameters (and over same time intervals; Figs. 3a–3d) as that for FN. Figure 3d shows the results 72 h after plating, where the cells displayed little concentration-dependent elongation or alignment. Statistical analysis of the orientation for cells in the high concentration region of the gradient (600–800 μm, but away from the edge itself) yielded a net orientation of 38 $\pm$ 3° whereas it was 6.3 $\pm$ 0.9° for cells on FN from the same concentration region. By convention, cells with orientation angles of less than 10° are considered to be highly aligned.[37] As both the specific FN and non-specific BSA gradients have the same topography, we concluded that the highly elongated and aligned morphology seen in Fig. 2d arises from the increased FN concentration in conjunction with the topography, and not from the contact guidance provided by the topography alone.

To further examine this issue, we also made a BSA gradient on a FN monolayer as well as a FN gradient on a FN monolayer and monitored cell alignment over a 24 h period at 6 h intervals. In the former case, we observed greater alignment of the fibroblasts than on the BSA gradient/BSA background construct, but the cells were mostly located *between* the BSA gradient fibers, where this structure having height of ~2 μm, seemingly formed a "fence" for the fibroblasts to locate in between and spread and migrate. By contrast,

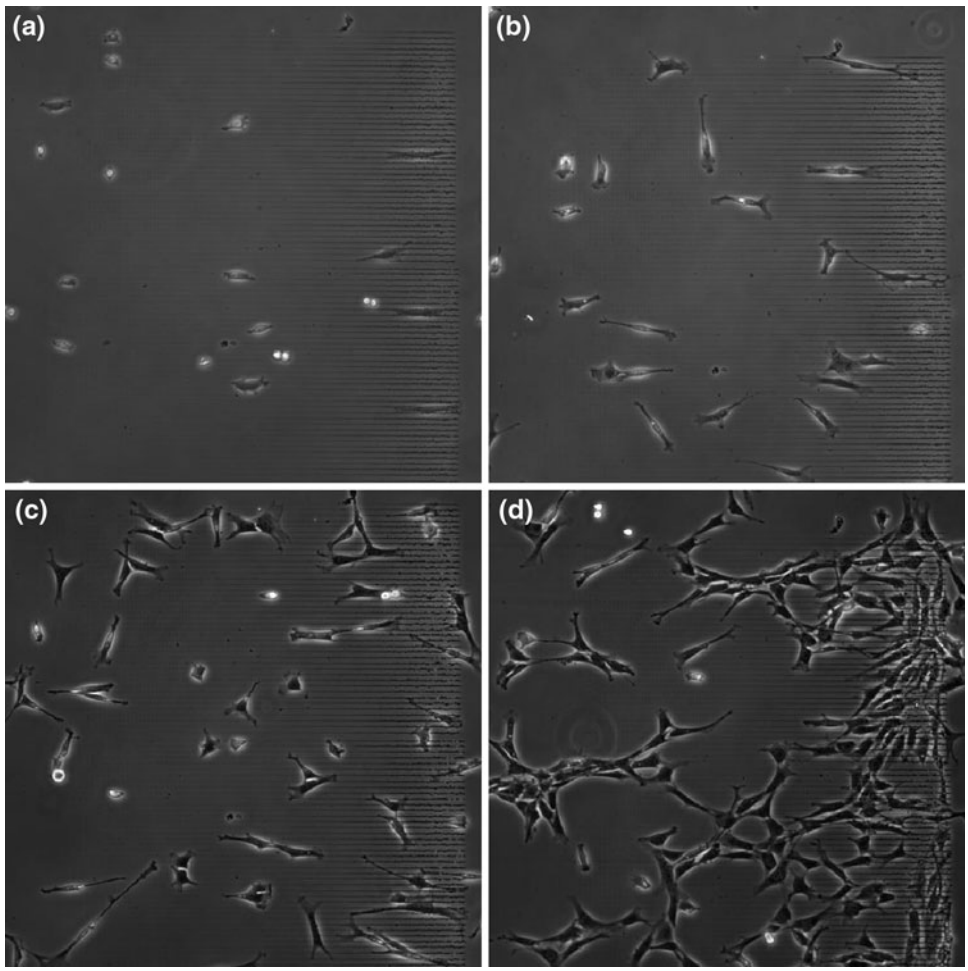

FIGURE 3. Phase contrast images at four time points of 5 (a), 24 (b), 48 (c), and 72 (d) h post-seeding for 3T3 fibroblasts on a BSA gradient made with the same design parameters as that shown in Fig. 1. The field size is the same as in Fig. 1.

far fewer cells were elongated on the BSA gradient structure itself, which is more typical of the usual sense of contact guidance. The FN/FN construct showed two types of behavior, where (i) some cells elongated along the crosslinked gradient, similar to the FN gradient/BSA background shown in Fig. 2, and (ii) some cells showed similar alignment behavior to the BSA gradient/FN background construct, where the cells were located in between the fabricated structures. In both cases, the results point to respective roles of contact guidance and ECM cues.

We note that the effect of soluble matrix ligands in the culture media on cell adhesion is small, as the fibroblasts showed minimal interaction with the BSA gradient on Day 1 relative to those on the FN gradient on the same BSA monolayer background. This is seen by comparing the images in Figs. 3a and 3b (BSA) with those in Figs. 2a and 2b (FN) at the same time points.

Given the large changes in elongation and alignment observed with increasing FN concentration, we next examined these morphological parameters at different local concentrations. To this end linear FN patterns with constant point densities of 0.1, 0.2, 0.3, and 0.4 points/μm were fabricated where these parameters corresponded to uniform concentrations of 1.32, 2.64, 3.96, and 5.28 μM, respectively (from the fit in Fig. 1b). Like the gradient design, the resulting linear fibers were 800 μm in length and separated by 10 μm. For reference, the corresponding concentrations points in the linear gradient are indicated by the arrows in Fig. 2c. Representative fields of view of adhered cells for these four concentrations are shown in the four panels in Fig. 4 (presented in order of increasing concentration). The fibroblast morphology and orientation on the linear fibers of constant concentration were similar to those at the corresponding points of the gradients, suggesting that the local concentration rather than change thereof is the dominant factor in the response to a gradient of this size scale.

To further investigate this issue, we next quantitatively characterized the elongation and orientation[29,37] of cells at these discrete concentrations. Figure 5a shows

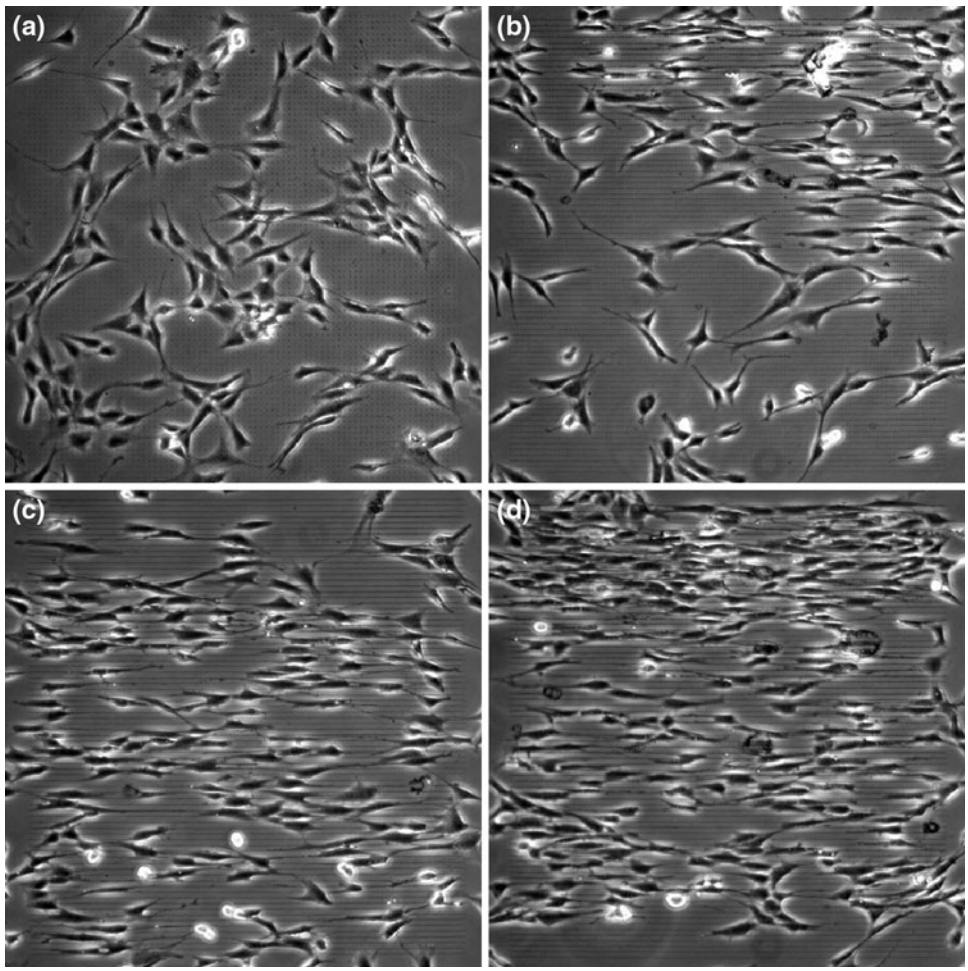

FIGURE 4. Phase contrast images of fabricated structures of uniform FN concentrations of 1.32 (a), 2.64 (b), 3.96 (c) and 5.28 (d) μM, 72 h post-plating. The field size is 800 μm.

the resulting data. Over this range the elongation was significantly affected by the FN concentration, where an increase of ~2 fold was observed between the lowest and highest points. The results for cells on the 3.96 μM ($n = 136$ cells), and 5.28 μM ($n = 129$) structures were statistically similar ($p = 0.37$) indicating a saturated response, where higher FN concentrations did not result in increased elongation. However, the elongation was greater ($p = 0.01$) for the 3.96 μM structure than for the 2.64 μM ($n = 92$) case. Similarly, this concentration resulted in greater elongation compared to the lowest FN concentration of 1.32 μM ($n = 126; p < 1 \times 10^{-5}$).

As shown in Fig. 5b, the FN concentration also significantly affected the fibroblast orientation. The orientation angle of the fibroblasts decreased markedly from the lowest (32°) to the highest concentration (9°), becoming increasingly aligned. The data for the 3.96 and 5.28 μM points were statistically similar ($p = 0.83$) indicating a saturated response at these concentrations, as was seen in the elongation analysis. However, the angle was decreased for the 3.96 μM structure relative to the 2.64 μM case ($p < 1 \times 10^{-5}$), which was likewise decreased relative to the lowest concentration (1.32 μM; $p = 0.007$). Collectively, the elongation and orientation data demonstrated the effect of the increasing FN concentration to elongate and orient the cells with respect to the FN linear axis.

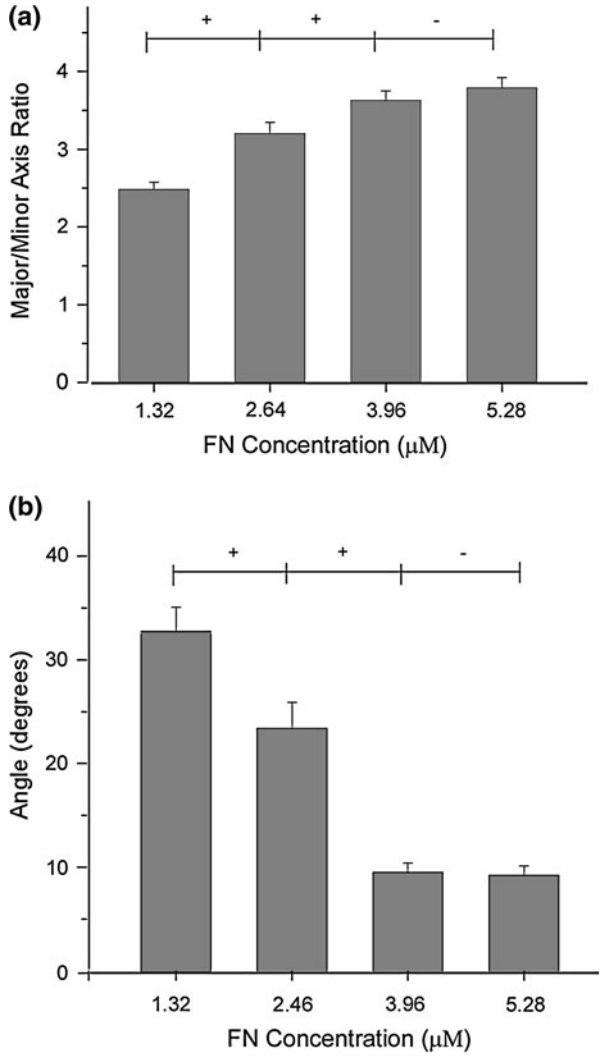

FIGURE 5. Morphological parameters for 3T3 fibroblasts (72 h post-plating) on the 4 FN concentrations shown in Fig. 3, where (a) and (b) are the elongation and orientation data, respectively, and statistical differences and similarities are denoted by (+) and (−), respectively.

Cytoskeletal Response

The cytoskeletal properties of adhered cells were modulated by the FN concentration in an analogous manner to that of the morphological data. Figure 6 gives representative phase contrast (left) and F-actin images (center) 36 h post-plating for three regions of an FN gradient (same design as in Figs. 1 and 2), corresponding to the length-scales of 200–400 μm (a), 400–600 μm (b), and 600–800 μm (c) which we will denote as corresponding to low, medium, and high concentration. The angular distribution of stress fibers relative to the FN axis was quantitated through the use of circular statistics (Eq. 1) and the resulting histograms for cells adhered on these length-scales are given in the right panel of Fig. 6. The distribution at the low concentration (Fig. 6a) was characterized by little angular preference, with many angles being represented, similar to that observed to the typical phenotype for these cells in culture. This distribution significantly narrowed at the medium (Fig. 6b) and high (Fig. 6c) concentrations where the stress fibers became highly aligned with the cell morphology along the axis of the FN. The resulting circular standard deviations for the low, medium, and high concentrations were 63.2, 19.8, and 13.2°, respectively. The pairwise Watson U^2 test indicated that the stress fiber orientations at all these concentrations were significantly different, with $p < 0.001$ for all comparisons.

The anti-vinculin immunofluorescence images of the focal adhesions are shown in Fig. 7. The left and right panels correspond to the raw images and those contrast enhanced, respectively, where the latter was done to simultaneously visualize the focal adhesions and the FN, where the fluorescence contrast in the latter arises from residual entrapped Rose Bengal. For all concentrations, some punctuate focal adhesions are associated with the FN features (see representative arrows in each case). At the highest concentration, some of the focal adhesions are seen at the leading and trailing edges, over-lapping the FN axis. While there was local overlap of the adhesions with the FN, we note that no

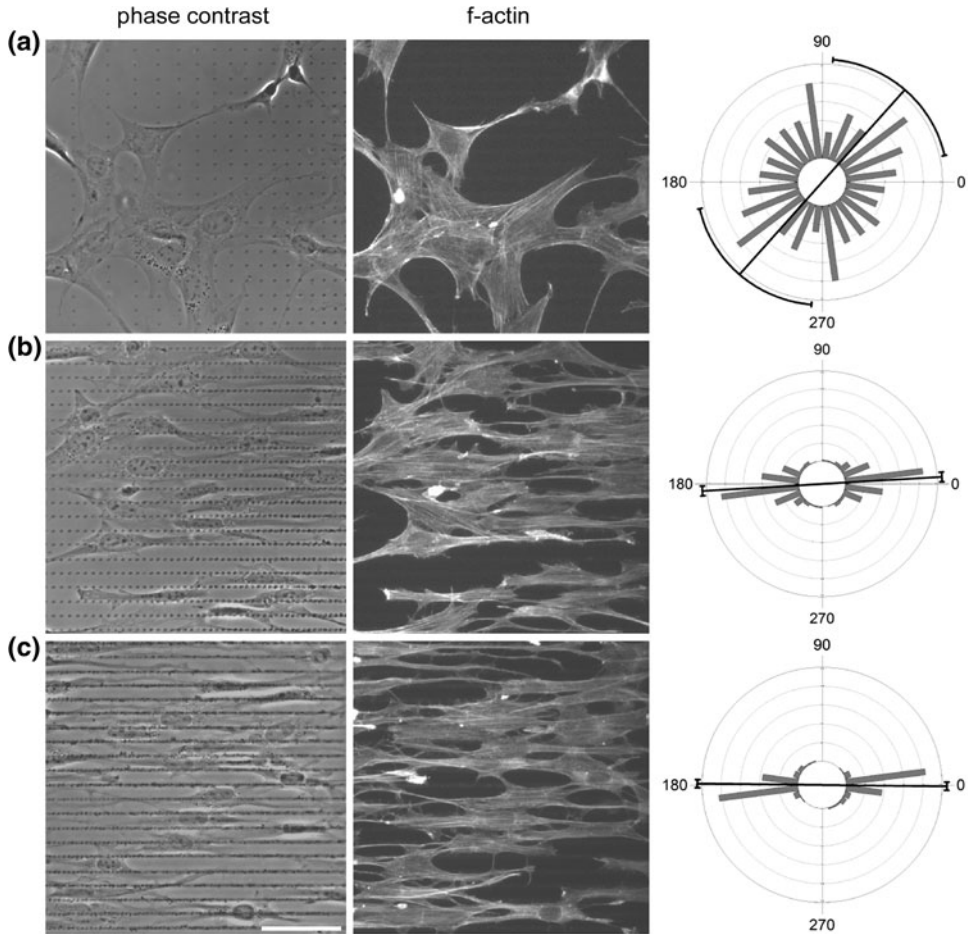

FIGURE 6. Phase contrast images and F-actin staining for low, medium, and high concentration regions of the FN gradient. The last column represents the resulting histogram of the circular statistical analysis in each case. The stress fibers become increasingly aligned as the topography becomes more continuous, rather than discrete points. Scale bar = 50 μm.

global correlation was found, as many of these assemblies were located between the FN fibers on the BSA background.

DISCUSSION

We have presented a new approach for the fabrication of 3D micro-structured covalently assembled protein gradients. An enabling aspect of the MPE approach is that the protein concentration can be changed without altering the topography, affording the ability to examine the roles of biochemical and spatial cues (separately and together) that contribute to the measured response. We further suggest this approach overcomes some limitations of previous synthetic methods to create insoluble gradients. For example, Plummer *et al.*[32] fabricated FN gradients through creating a gradient of deposited gold unto which FN was covalently bound. They observed preferential fibroblast attachment to higher concentrations, however, the pattern was 2 dimensional and the FN was not linked together. Photocrosslinking of the FN as achieved through the MPE technique may be more biomimetic.

Our approach also provides increased mechanical stability. This is evidenced by the observation that after 3 days in culture, based on phase contrast and fluorescence imaging, the gradients showed no clear degradation (not shown). Additionally, the fabricated structures are mechanically robust with respect to either water flow or dehydration/rehydration. This stability arises because the fabricated protein structures are covalently linked to each other and to the BSA monolayer, which is then strongly adsorbed to the organosilane monolayer, which is covalently bound to the glass substrate. In contrast, in microcontact printing, protein molecules adhere to each other and to the substrate *via* much weaker Van de Waals forces.

The microscope-based approach further permits the synthesis of structures with sub-micron topographic

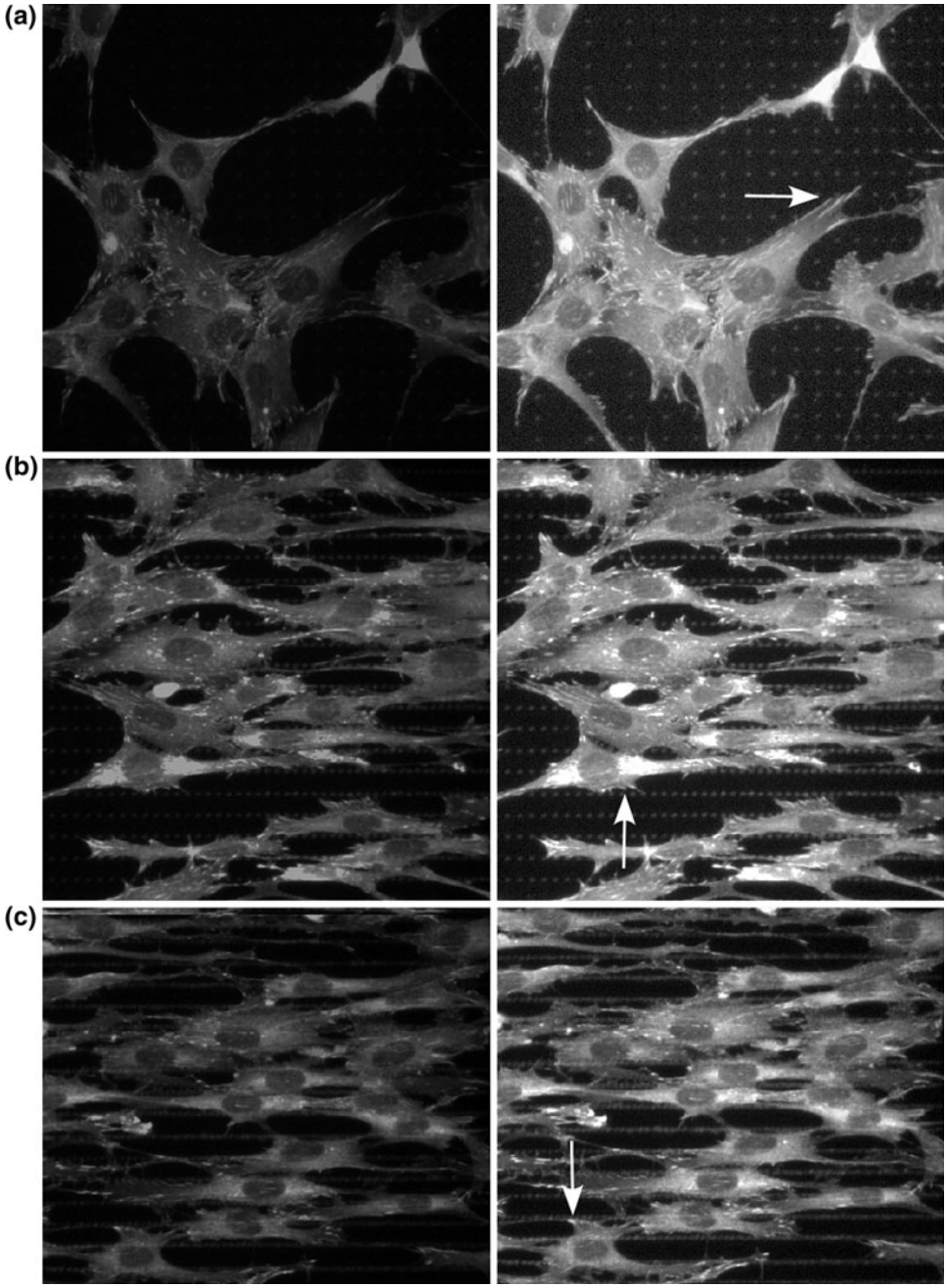

FIGURE 7. Focal adhesion staining for the same cells as shown in Fig. 6, where the left and right panels are the raw and contrast stretched (to simultaneously visualize the focal adhesions and the crosslinked FN) data, respectively. The FN fluorescence contrast arises from residual entrapped photoactivator. The arrows denote representative overlap of the focal adhesions with the crosslinked FN.

features, presenting cells with analogous topographic cues that are present in the native ECM. Moreover, since full length purified proteins are used cell integrins are exposed to the appropriate protein binding sites, e.g., the RGD/PHSRN sequences on FN. For example, in prior work, through the "stick and grip" method,[17] we observed that the β_1 integrin was active in dermal fibroblast binding to MPE fabricated FN structures (unpublished results). Additionally, we found high specificity of the monoclonal HFN7.1 antibody to MPE crosslinked human FN.[29]

While our long-term motivation lies in tissue engineering applications, here we focused our attention on studying the fundamental cell–matrix interactions. Specifically the FN gradients were used as substrates to compare the fibroblast response to changing protein

concentrations in the presence of micro-structured topography. This is of interest as the role of concentration gradients on cell response is not completely understood. For example, using immobilized gradients created through microfluidics, Kenis and co-workers[18,19] showed that the primary factor in governing cell migration was the local concentration, rather than the concentration slope. In contrast, other reports have cited the importance of local slope.[5] Our data for 3T3 fibroblasts on FN suggests the importance of local concentration, as the cell orientation and elongation at the constant concentrations (representative images and analysis in Figs. 4 and 5 respectively), were similar to those observed on the gradient (Fig. 2).

We note that the net fibroblast response further depends on the combination of topographic features and protein concentration. While some alignment exists for cells on the BSA gradient, which provided only topographic cues, this is a weak effect compared to FN, where the average orientation angles were 38 and 6° respectively. In strong contrast, the alignment and elongation data for the cells shown in Figs. 4b and 4d were statistically different although the topographies were similar (continuous linear structures of the same height and width) but with different FN concentrations, revealing the contribution of the ECM cues. The examples of using a BSA gradient/FN background and FN gradient/FN background further showed how contact guidance and ECM cues can operate together and separately. By contrast, other reports documented that the morphological and cytoskeletal properties of cells on submicron patterned structures resulted primarily from contact guidance. For example, Nealey and co-workers[37,38] reported that both epithelial cells and keratocytes showed a high degree of alignment on silicon grooves and ridges. They also observed highly aligned stress fibers but cells had fewer focal adhesions relative to those adhered distally to the etched patterns.

While we did not find a global statistically significant correlation between the spatial distribution of focal adhesions and FN fibers (with respect to total expression), some focal adhesions were co-localized with the FN structures (examples denoted by arrows in Fig. 7). It was not expected that the focal adhesions would be solely located on the FN as the BSA monolayer is not a repulsive background and the cells will eventually form new adhesions. This is a different scenario than sometimes reported in the literature where islands or stripes of attractive regions were placed against a cell-repulsive background, and the focal adhesions are expressed solely on the fabricated regions by default.[14,16] This observation is consistent with our prior work which showed that the distribution of focal adhesions of fibroblasts adhered on crosslinked BSA microfibers were randomly distributed between these features.[29] Our data taken in conjunction with that of Nealey is suggestive that the stress fiber alignment may primarily result from the topographic response, whereas the focal adhesion distribution arises from a combination of topographic and ECM cues.

We need to also consider the role of feature size and spacing on the resulting cell morphology and cytoskeletal features. As the instrument is microscope-based, and MPE is a threshold process, the size of the fabricated features cannot be significantly increased. Specifically, we have not been able to achieve efficient photocrosslinking at lower resolution (which would yield larger fabricated features) than the optics that were used here (0.5 NA), which resulted in lateral diameters of about 700 nm. However, comparisons can be drawn to recent work by Doyle *et al.*[14] Through a combination of printing and ablation, they created 1D "stripes" of varying widths (1–40 μm) from FN and examined the spreading of 3T3 fibroblasts. For cells on thinner stripes (e.g., 1 μm) they observed a similar uniaxial phenotype to that shown here at high FN concentration. When the widths became larger than the cell size, this elongation was decreased and the morphology approached the typical fibroblast behavior seen on monolayers or in culture. In terms of fiber spacing, we previously showed that when FN and fibrinogen fibers (~700 nm width) were spaced by distances much larger than cell diameters, i.e., 40 μm, the effects of alignment and elongation of fibroblasts were decreased relative to those adhered to fibers spaced by 10 μm (~one cell diameter).[29]

CONCLUSIONS

We have demonstrated the fabrication of micro-structured covalently linked FN gradients and have achieved a large dynamic range (~4 fold) where the design allows studying the roles of topographic and ECM cues, separately and together, on fibroblast adhesion/spreading dynamics. We found that higher concentrations of FN with the same topography resulted in greater elongation and alignment, whereas these responses due to contact guidance provided by a BSA gradient were much less pronounced. While more work remains to fully understand how gradients of ECM proteins affect cell–matrix interactions, our current results suggest that contact guidance and integrin binding together and separately need to be considered in the substrate design for fundamental cell biology studies or eventual tissue engineering applications. We further suggest our design overcomes some of the limitations with other methods in terms of 3D

flexibility and may be more biomimetic. While for the purpose of development the gradients were fabricated on BSA surfaces, we note that they could be used to modify an existing 3D substrate.

ACKNOWLEDGMENTS

We gratefully acknowledge support under NIH 1U54-RR022232 and NSF CBET–1057766. Y.-D. Su and S.-J. Chen acknowledge support from National Cheng Kung University. We also thank Prof. Vladimir Rodionov for the use of the imaging system for live cell studies.

REFERENCES

[1]Basu, S., and P. J. Campagnola. Properties of crosslinked protein matrices for tissue engineering applications synthesized by multiphoton excitation. *J. Biomed. Mater. Res.* 71A(2):359–368, 2004.

[2]Basu, S., L. P. Cunningham, G. Pins, K. Bush, R. Toboada, A. R. Howell, J. Wang, and P. J. Campagnola. Multiphoton excited fabrication of collagen matrices crosslinked by a modified benzophenone dimer: bioactivity and enzymatic degradation. *Biomacromolecules* 6:1465–1474, 2005.

[3]Basu, S., C. W. Wolgemuth, and P. J. Campagnola. Measurement of normal and anomalous diffusion of dyes within protein structures fabricated via multi-photon excited crosslinking. *Biomacromolecules* 5:2347–2357, 2004.

[4]Belisle, J. M., J. P. Correia, P. W. Wiseman, T. E. Kennedy, and S. Costantino. Patterning protein concentration using laser-assisted adsorption by photobleaching, LAPAP. *Lab Chip* 8(12):2164–2167, 2008.

[5]Brandley, B. K., and R. L. Schnaar. Tumor cell haptotaxis on covalently immobilized linear and exponential gradients of a cell adhesion peptide. *Dev. Biol.* 135(1):74–86, 1989.

[6]Burdick, J. A., A. Khademhosseini, and R. Langer. Fabrication of gradient hydrogels using a microfluidics/photopolymerization process. *Langmuir* 20(13):5153–5156, 2004.

[7]Campagnola, P. J., A. R. Howell, D. Delguidas, G. A. Epling, J. D. Pitts, and S. L. Goodman. 3-Dimensional sub-micron polymerization of acrylamide by multiphoton excitation of xanthene dyes. *Macromolecules* 33:1511–1513, 2000.

[8]Chen, X., M. A. Brewer, C. Zou, and P. J. Campagnola. Adhesion and migration of ovarian cancer cells on crosslinked laminin fibers nanofabricated by multiphoton excited photochemistry. *Integr. Biol.* 1:469–476, 2009.

[9]Cunningham, L. P., M. P. Veilleux, and P. J. Campagnola. Freeform multiphoton excited microfabrication for biological applications using a rapid prototyping CAD-based approach. *Opt. Express* 14:8613–8621, 2006.

[10]Dalby, M. J., M. O. Riehle, D. S. Sutherland, H. Agheli, and A. S. Curtis. Fibroblast response to a controlled nanoenvironment produced by colloidal lithography. *J. Biomed. Mater. Res.* 69A(2):314–322, 2004.

[11]DeLong, S. A., A. S. Gobin, and J. L. West. Covalent immobilization of RGDS on hydrogel surfaces to direct cell alignment and migration. *J. Controlled Release* 109(1–3): 139–148, 2005.

[12]DeLong, S. A., J. J. Moon, and J. L. West. Covalently immobilized gradients of bFGF on hydrogel scaffolds for directed cell migration. *Biomaterials* 26(16):3227–3234, 2005.

[13]Dertinger, S. K., X. Jiang, Z. Li, V. N. Murthy, and G. M. Whitesides. Gradients of substrate-bound laminin orient axonal specification of neurons. *Proc. Natl Acad. Sci. USA* 99(20):12542–12547, 2002.

[14]Doyle, A. D., F. W. Wang, K. Matsumoto, and K. M. Yamada. One-dimensional topography underlies three-dimensional fibrillar cell migration. *J. Cell Biol.* 184(4):481–490, 2009.

[15]Fricke, R., P. D. Zentis, L. T. Rajappa, B. Hofmann, M. Banzet, A. Offenhausser, and S. H. Meffert. Axon guidance of rat cortical neurons by microcontact printed gradients. *Biomaterials* 32(8):2070–2076, 2011.

[16]Gallant, N. D., K. E. Michael, and A. J. Garcia. Cell adhesion strengthening: contributions of adhesive area, integrin binding, and focal adhesion assembly. *Mol. Biol. Cell* 16(9):4329–4340, 2005.

[17]Garcia, A. J., and N. D. Gallant. Stick and grip: measurement systems and quantitative analyses of integrin-mediated cell adhesion strength. *Cell Biochem. Biophys.* 39(1):61–73, 2003.

[18]Gunawan, R. C., E. R. Choban, J. E. Conour, J. Silvestre, L. B. Schook, H. R. Gaskins, D. E. Leckband, and P. J. Kenis. Regiospecific control of protein expression in cells cultured on two-component counter gradients of extracellular matrix proteins. *Langmuir* 21(7):3061–3068, 2005.

[19]Gunawan, R. C., J. Silvestre, H. R. Gaskins, P. J. Kenis, and D. E. Leckband. Cell migration and polarity on microfabricated gradients of extracellular matrix proteins. *Langmuir* 22(9):4250–4258, 2006.

[20]Isenberg, B. C., P. A. Dimilla, M. Walker, S. Kim, and J. Y. Wong. Vascular smooth muscle cell durotaxis depends on substrate stiffness gradient strength. *Biophys. J.* 97(5):1313–1322, 2009.

[21]Jeon, N. L., S. K. W. Dertinger, D. T. Chiu, I. S. Choi, A. D. Stroock, and G. M. Whitesides. Generation of solution and surface gradients using microfluidic systems. *Langmuir* 16(22):8311–8316, 2000.

[22]Kaehr, B., R. Allen, D. J. Javier, J. Currie, and J. B. Shear. Guiding neuronal development with in situ microfabrication. *Proc. Natl Acad. Sci. USA* 101(46):16104–16108, 2004.

[23]Kaunas, R., P. Nguyen, S. Usami, and S. Chien. Cooperative effects of Rho and mechanical stretch on stress fiber organization. *Proc. Natl Acad. Sci. USA* 102(44):15895–15900, 2005.

[24]LaFratta, C. N., D. Lim, K. O'Malley, T. Baldacchini, and J. T. Fourkas. Direct laser patterning of conductive wires on three-dimensional polymeric microstructures. *Chem. Mater.* 18(8):2038–2042, 2006.

[25]Mai, J., L. Fok, H. Gao, X. Zhang, and M. M. Poo. Axon initiation and growth cone turning on bound protein gradients. *J. Neurosci.* 29(23):7450–7458, 2009.

[26]Maruo, S., O. Nakamura, and S. Kawata. Three-dimensional microfabrication with two-photon-absorbed photopolymerization. *Opt. Lett.* 22:132–134, 1997.

[27]Mooney, J. F., A. J. Hunt, J. R. McIntosh, C. A. Liberko, D. M. Walba, and C. T. Rogers. Patterning of functional antibodies and other proteins by photolithography of silane

monolayers. *Proc. Natl Acad. Sci. USA* 93(22):12287–12291, 1996.
[28]Neckers, D. C. Rose Bengal. *J. Photochem. Photobiol. A* 47:1–29, 1989.
[29]Pins, G. D., K. A. Bush, L. P. Cunningham, and P. J. Campagnola. Multiphoton excited fabricated nano and micropatterned extracellular matrix proteins direct cellular morphology. *J. Biomed. Mater. Res.* 78A:194–204, 2006.
[30]Pitts, J. D., P. J. Campagnola, G. A. Epling, and S. L. Goodman. Reaction efficiencies for sub-micron multiphoton freeform fabrications of proteins and polymers with applications in sustained release. *Macromolecules* 33:1514–1523, 2000.
[31]Pitts, J. D., A. R. Howell, R. Taboada, I. Banerjee, J. Wang, S. L. Goodman, and P. J. Campagnola. New photoactivators for multiphoton excited three-dimensional submicron cross-linking of proteins: bovine serum albumin and type 1 collagen. *Photochem. Photobiol.* 76(2):135–144, 2002.
[32]Plummer, S. T., Q. Wang, P. W. Bohn, R. Stockton, and M. A. Schwartz. Electrochemically derived gradients of the extracellular matrix protein fibronectin on gold. *Langmuir* 19(18):7528–7536, 2003.
[33]Rhoads, D. S., and J. L. Guan. Analysis of directional cell migration on defined FN gradients: role of intracellular signaling molecules. *Exp. Cell Res.* 313(18):3859–3867, 2007.
[34]Slater, J. H., and W. Frey. Nanopatterning of fibronectin and the influence of integrin clustering on endothelial cell spreading and proliferation. *J. Biomed. Mater. Res. A* 87A(1):176–195, 2008.
[35]Sridhar, M., S. Basu, V. L. Scranton, and P. J. Campagnola. Construction of a laser scanning microscope for multiphoton excited optical fabrication. *Rev. Sci. Instrum.* 74(7):3474–3477, 2003.
[36]Swartz, M. A. Signaling in morphogenesis: transport cues in morphogenesis. *Curr. Opin. Biotechnol.* 14(5):547–550, 2003.
[37]Teixeira, A. I., G. A. Abrams, P. J. Bertics, C. J. Murphy, and P. F. Nealey. Epithelial contact guidance on well-defined micro- and nanostructured substrates. *J. Cell Sci.* 116:1881–1892, 2003.
[38]Teixeira, A. I., P. F. Nealey, and C. J. Murphy. Responses of human keratocytes to micro- and nanostructured substrates. *J. Biomed. Mater. Res.* 71A(3):369–376, 2004.
[39]von Philipsborn, A. C., S. Lang, J. Loeschinger, A. Bernard, C. David, D. Lehnert, F. Bonhoeffer, and M. Bastmeyer. Growth cone navigation in substrate-bound ephrin gradients. *Development* 133(13):2487–2495, 2006.
[40]Wang, S., C. Wong Po Foo, A. Warrier, M. M. Poo, S. C. Heilshorn, and X. Zhang. Gradient lithography of engineered proteins to fabricate 2D and 3D cell culture microenvironments. *Biomed. Microdevices* 11(5):1127–1134, 2009.